High-Performance All-Carbon Yarn Micro-Supercapacitor for an Integrated Energy System

Qinghai Meng, Haiping Wu, Yuena Meng, Ke Xie, Zhixiang Wei, and Zhengxiao Guo*

Yarn micro-supercapacitors with high performance, flexibility and deformability are essential for integration with portable and wearable electronics.[1,2] Considerable progress has been made in recent years, in terms of fiber supercapacitors and intergrated fiber solar cells with supercapacitors.[3–8] As a widely used electrode material in the field of energy storage, carbon nanotubes (CNTs) possess excellent physical and chemical properties, such as excellent electrical and thermal conductivities, mechanical properties and chemical stabilities.[6,9–11] By means of dry and wet spinning methods, continuous carbon nanotubes yarn has been spun,[12–14] which greatly promotes the development of yarn micro-supercapacitors. Carbon based micro-supercapacitors show little reduction in capacitance even after hundreds of thousands of charge-discharge cycles.[8,15,16] However, the application of CNT yarn based micro-supercapacitors is limited by low capacitance since the large specific surface area of CNTs is not effectively utilized. Clearly, this major drawback limits the use of the CNT yarn based micro-supercapacitors as power sources for electronic textiles. The introduction of pseudocapacitance materials such as conducting polymers significantly improves capacitance.[17–20] However, such composite supercapacitors suffer from decreased cycling stability because the active material swells and shrinks during the doping-dedoping process.[21,22] The introduced active materials also affect the electrical conductivities of the electrode. Increase the capacitance and energy density without sacrificing high cycling stability remains a challenge in carbon-based yarn micro-supercapacitors.

In the work presented here, we describe the design and fabrication of flexible and efficient all-carbon based yarn micro-supercapacitors. Using a wet-spinning method, single-walled carbon nanotubes (SWNT) and chitosan (CHI) composite yarn was prepared. After thermal treatment at high temperature, chitosan was carbonized, and a composite yarn electrode containing SWNT and active carbon (SWNT@C) was produced. The as-prepared electrode is rich in mesopores, which is more favorable for the transport and storage of charges. The active carbon on the surface of SWNT bundles not only provides a relatively large specific surface area of electrode material but also acts as the binder between the crossed SWNT bundles to improve the yarn electrical conductivity. This unique structure leads to high capacitance, high energy density and excellent cycling stability in the resulting SWNT@C electrode based yarn micro-supercapacitor. As shown in **Figure 1**a, a home-made apparatus based on a wet-spinning method was built to fabricate single-walled carbon nanotubes and chitosan (SWNT@CHI) composite yarn. SWNT dispersions and chitosan solutions were prepared as described in the Experimental section. We tried to reduce the impurity contents in the SWNT dispersion to obtain yarn of high performance. However, the key issue of the wet-spinning method is to ensure uniformity of the SWNT dispersion. We studied the effect of sodium deoxtcholate concentrations (SDC) on the uniformity of SWNT dispersions. A homogeneous dispersion was obtained if the mass ratio of SDC and SWNT was larger than 1:1.5. Figure 1b shows the state of SWNT in its dispersion, and no agglomeration or precipitation was observed. Scanning Electron Microscopy (SEM) images with different concentrations of SDC dispersion deposited on silicon wafers are shown in Figure S1 in Supporting Information. Although uniform dispersion is obtained at different concentration of SDC, but a high content of SDC is unfavourable for high performance yarn. At a mass ratio of 1:1.5 of SDC to SWNT, a homogeneous dispersion with low impurity content was obtained (Figure S1c). At a smaller amount of SDC, a large amount of agglomerates has formed (Figure S1d). Therefore, the finally selected spinning dispersion contained 4 mg mL^{-1} of SWNT and 2.7 mg mL^{-1} SDC, typically. The syringes were driven by a double-channel syringe pump. Spinning dispersion was injected into a co-flowing CHI solution, and a SWNT@CHI yarn was formed as a result of coagulation of SWNT. From the homogeneous SWNT dispersion, we obtained continuous composite yarns successfully (Figure 1c). The diameter of the yarn is tunable by regulating the size of spinneret tip and the ratios of the relative flowing speed of spinning and coagulation solutions. The yarn has a thin outer shell of CHI and a core of SWNT bundles. As reported before, the SWNTs in the yarn are slightly oriented along the axial direction as a result of shear induced during injection.[23] As water diffuses through the outer CHI shell, the interior SWNT coagulate. Besides, the surface of yarns collapse and form gully-like structure during the drying process. Figure 1d shows the SEM image of an as-prepared yarn, the morphology of which is consistent with the above description. The yarn possesses excellent flexibility after exhaustively drying in air. As shown in Figure 1e, a pair-knot was tied to demonstrate that. Besides, if the dried yarn was moistened again, it can be bent into any

Q. H. Meng, Dr. H. P. Wu, Dr. Y. N. Meng, K. Xie, Prof. Z. X. Wei
National Center for Nanoscience and Technology
Beijing 100190, PR China
E-mail: weizx@nanoctr.cn
Prof. Z. X. Guo
Department of Chemistry
University College London
London WC1H 0AJ, UK

DOI: 10.1002/adma.201400399

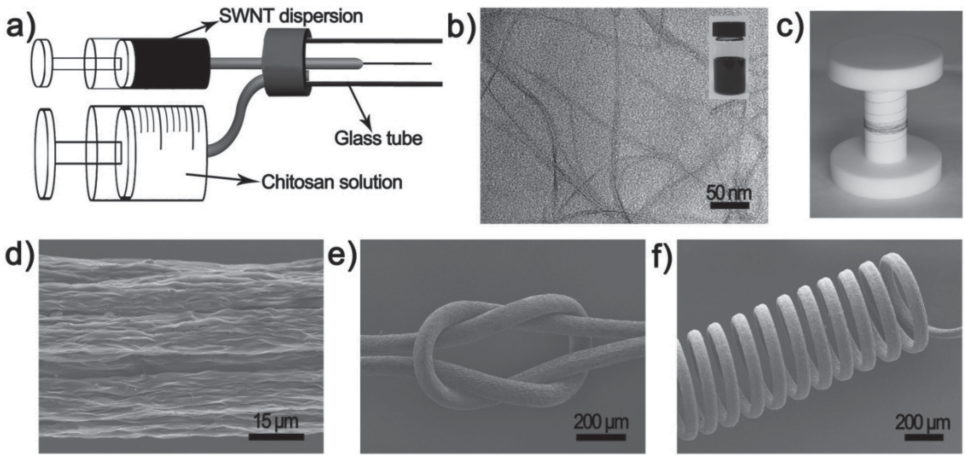

Figure 1. a) The spinning apparatus for the fabrication of continuous SWNT yarns. b) The TEM image of the state of SWNT in dispersion (insert image is the photo image of SWNT dispersion in a lab glassware). c) Digital image of SWNT@CHI yarns wound on a Teflon reel. d) SEM image of the surface of as-prepared SWNT@CHI yarns. e) SWNT@CHI yarn tied in a pair-knot indicating the excellent flexibility. f) A yarn made spring with no deformation after dried.

shape, which is retained after subsequent drying. A SWNT yarn spring was made in such a way (Figure 1f).

Poly(vinyl alcohol) solution is a commonly used coagulating bath in some previous reports.[23–26] However, most of the coagulating constituent was adsorbed on the surface of yarn, which accordingly reduces the yarn's electrical conductivity. Surprisingly, a relatively small amount of chitosan was adsorbed on the surface of yarn in the wet-spinning process (see Figures S2a & b in Supporting Information). This greatly improves the electrical conductivity of yarn. CHI is a polysaccharide like cellulose, the similarity between CHI and cellulose structure indicates great potential for producing active carbon.[27–30] By means of carbonization of the SWNT@CHI yarn, we obtained a SWNT@C yarn with high electrical conductivity. **Figure 2** shows the morphology of a SWNT@C yarn. Compared with the SWNT@CHI yarn (Figure S2a and b in Supporting Information), the protrusion on the surface of the SWNT@C yarn changes from ravine-like to flake-like structure. The change of morphology improves the specific surface area of yarn. In SWNT@CHI yarn, intricate bundles of SWNT were buried in chitosan. When forming SWNT@C yarn, the SWNT act as a framework in the process of carbonization of chitosan. Figure 2c gives the mophology of a cross-section of the yarn. SWNT bundles with diameters of ca. 20~30 nm can be seen clearly, and SWNT bundles distribute loosely from surface to interior of the yarn. The enlarged image of cross-section is shown in Figure S2c. Besides, the surface of the yarn show a stacked reticular structure (Figure 2d). Generally, SWNT yarn spinned from a SWNT forest (dry-spinning method) have a compact structure. Although the compact structure promises high electrical conductivities, it does not utilize the large specific surface area of SWNT. In contrast, the loose structure of the as-prepared yarn is also high conductive due to the interconnected SWNT bundles, and have high surface area due to loosely compacted SWNT bundles. Just as porous materials, the loose structure shows a significant improvement on the capacitance of micro-supercapacitors prepared by this material. Figure S3a shows the nitrogen adsorption/desorption isotherms of SWNT@C yarn. The Brunauer–Emmett–Teller (BET) result shows the specific area of SWNT@C is 268 $m^2 g^{-1}$. Besides, the pore-size distribution reveals that the pore size is mainly in the range of mesoporous range (See Figure S3b in Supporting Information). We also conducted the mechanical performance test (the results are shown in Figure S3c in Supporting Information)). The fracture strength of SWNT@C yarn is 76 MPa, which is lower than that of SWNT@CHI (110 MPa). The possible explanation is that the SWNT@CHI yarn is filled with plastic polymer (CHI), however, after thermal treatment, interspace emerged when CHI converts to rigid carbon and the tensile strength of SWNT@C yarn turns small. From this perspective, the Young's modulus of SWNT@C yarn should larger than that of SWNT@CHI yarn as the plastic polymer is replaced by rigid carbon. According to the stress-strain curve, the Young's modulus of SWNT@C yarn is 10.9 GPa, while for SWNT@CHI yarn, the value is 1.5 GPa. This is consistent with the explanation mentioned above.

However, it is hard to distinguish active carbon resulted from the carbonization of CHI from SEM or transmission electron microscopy (TEM). X-ray photoelectron spectroscopy (XPS) and Raman measurements were conducted to investigate the forementioned matter. The typical XPS wide scan spectra of the SWNT@C yarn and the SWNT sample are shown in Figure S4. Both spectra show definite carbon and oxygen peaks, representing the major constituents of the sample surface. The XPS C1s spectrum of the samples could be deconvoluted into five peaks (SWNT@C yarn) and four peaks (SWNT sample), respectively, resulting from the introduction of active carbon in the SWNT@C yarn (Figure 2e). Both samples exhibit a main peak at 284.65 eV, which can be attributed to the sp2-hybridized graphite-like carbon atoms. The peaks at 285.01 eV, is assigned to the sp3-hybridized carbon.[31,32] Compare the XPS data of the SWNT sample with the SWNT@C yarn, the intensity ratio of sp2/sp3 increases from 2.57 to 4.15, revealing the introduction of active carbon resulted from the carbonization of CHI. Figure 2f shows the Raman spectrum of SWNT@C yarn and SWNT sample. The typical peaks

ADVANCED MATERIALS
www.advmat.de

www.MaterialsViews.com

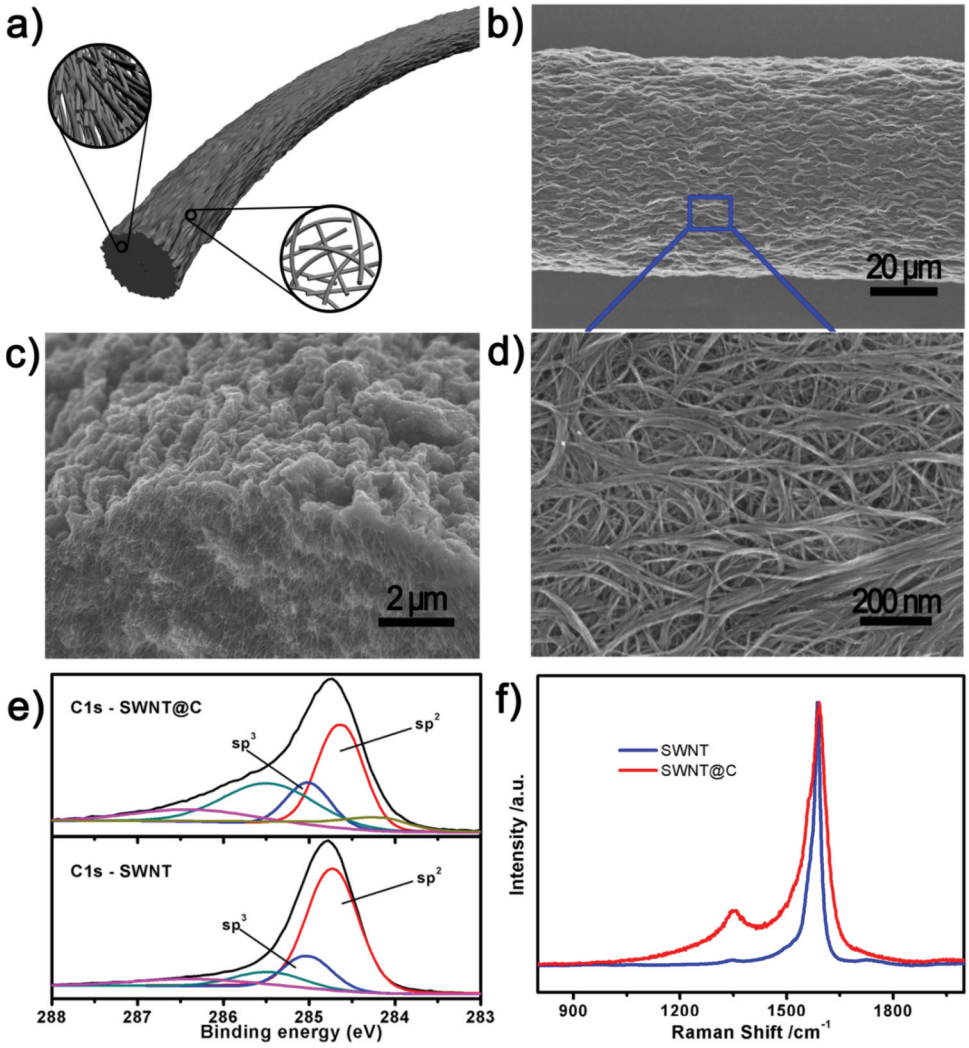

Figure 2. a) The illustration of morphology of SWNT@C yarn. b) The SEM image of SWNT@C yarn after calcining. c) The SEM image of the cross section of SWNT@C yarn. d) The SEM image of the surface of SWNT@C yarn at high magnification. e) XPS C1s spectra of carbon sp^2/sp^3 analysis. f) Raman spectroscopy of SWNT samples and SWNT@C yarn.

at 1348 cm^{-1} and 1592 cm^{-1} reveals the D-band and G-band of SWNT, and the intensity ratio of ID/IG is usually used to characterize the defects and disorder in SWNT samples.[33–36] According to the data in Figure 2f, this value reduces from 45.45 (SWNT) to 4.76 (SWNT@C). The result is consistent with the XPS result mentioned above, and reveals the existence of active carbon in the SWNT@C yarn.

We conducted electrochemical measurements of yarn micro-supercapacitors using a PVA/H_2SO_4 gel electrolyte. The yarn micro-supercapacitors were fabricated and characterized as described in the Experimental section. The two-yarn electrodes were clung together with the sticky gel electrolyte. The gel is used as a binder, a separator and the electrolyte. Because of the large viscosity of the gel, the two-yarn electrodes are closely contact. The electrochemical characterization of the SWNT@CHI and the SWNT@C yarn based micro-supercapacitors were investigated by cyclic voltammograms (CV) at a scan rate of 20 mV s^{-1} (**Figure 3**a). Obviously, typical rectangular shapes, which suggest a mechanism of electrochemical double layer capacitor, are obtained for both the materials. The SWNT@C yarns make full use of the specific surface area of the SWNT, which was expected to increase the capacity. As described above, the current density of the SWNT@C yarn is much higher than that of the SWNT@CHI. Figure 3b shows the CV curves of the SWNT@C yarn micro-supercapacitor at different scan rates (from 2 to 200 mV s^{-1}), indicating a good electrochemical stability and a very rapid response on voltage reversal.

The galvanostatic charge-discharge and the impedance spectrum measurements were also conducted to characterize the electrochemical capacitor performance of the yarn micro-supercapacitors. Figure 3c shows the charge-discharge curves of both yarn-based micro-supercapacitors at a current density of 0.1 mA cm^{-2}. It is noted that the large capacitance of the SWNT@C based capacitors originates from effective ion adsorption at the SWNT surface. Besides, both type of the micro-supercapacitors show nearly symmetrical charge and discharge curves, which also indicate the as-prepared device possesses a high reversibility.

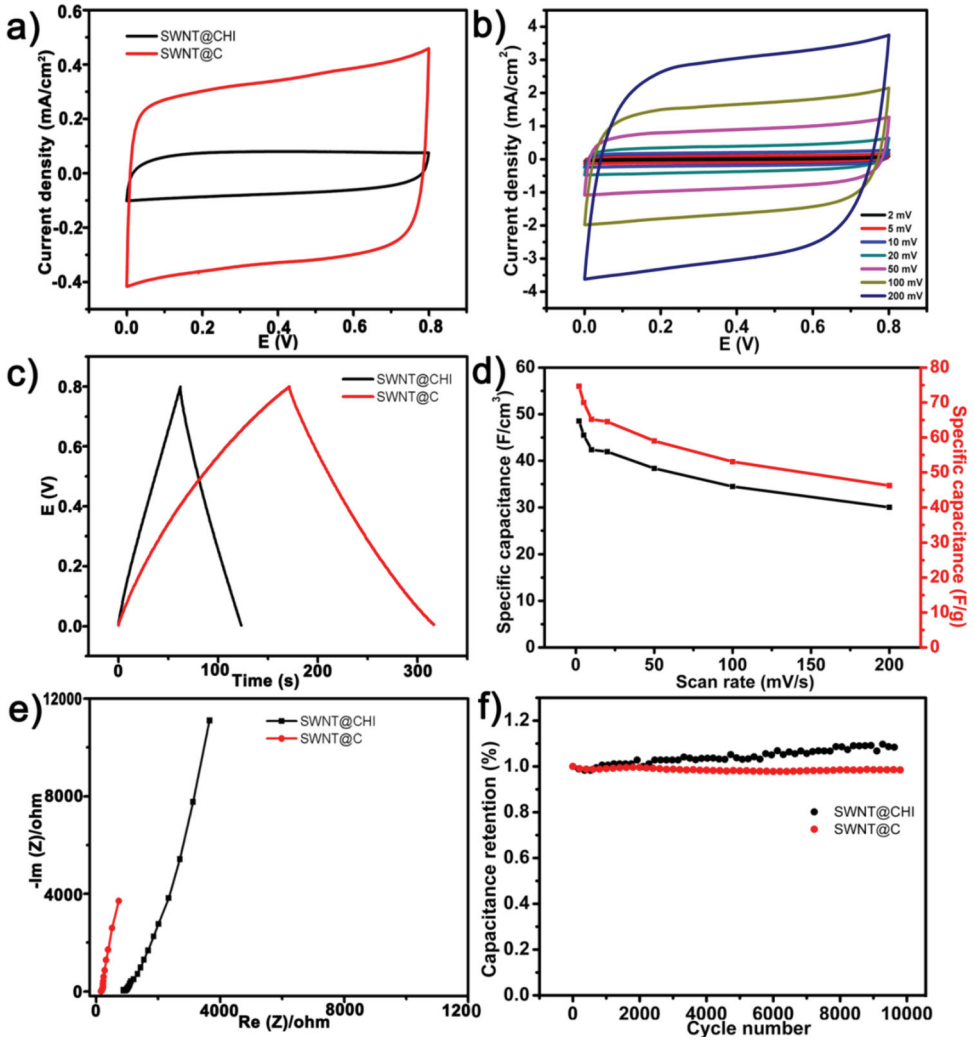

Figure 3. Electrochemical properties of the yarn micro-supercapacitors. a) Cyclic voltammograms of SWNT@CHI and SWNT@C yarn micro-supercapacitors at the scan rate of 20 mV s^{-1}. b) Cyclic voltammograms of SWNT@C yarn micro-supercapacitor at different scan rate. c) Galvanostatic charge/discharge curves of SWNT@CHI and SWNT@C yarn supercapacitor at 0.1 mA cm^{-2}. d) Volumetric and mass capacitance as a function of scan rate for SWNT@C yarn. e) Electrochemical impedance spectroscopy with a frequency loop from 50 kHz to 10 mHz. f) The long-term cycling stability.

The volumetric and mass capacitances were further studied as a function of scan rate from 2 to 200 mV s^{-1} for the SWNT@CHI and the SWNT@C micro-supercapacitors (see Figures S5a & 3d). At a scan rate of 2 mV s^{-1}, the volumetric capacitance is 48.5 and 10.1 F cm^{-3} for the SWNT@C and the SWNT@CHI devices, respectively. Even at a scan rate of 200 mV s^{-1}, the capacitances can still maintain 30 and 4.4 F cm^{-3}, respectively for the two devices. The capacitances of the SWNT@C is at least 15 times higher than that reported previously on carbon-based electrodes (typically less than 3.05 F cm^{-3}).[15,37] Take the whole device into account, Lee et al.[6] showed the PEDOT/MWNT/Pt yarn based supercapacitors possesses a capacitance of 13 F cm^{-3}, which is only a third of that of the micro-supercapacitor presented here. Besides, the gravimetric capacitance of the SWNT@CHI and the SWNT@C devices are 6.6 F g^{-1} to 74.6 F g^{-1}, respectively, at the scan rate of 2 mV s^{-1}. The capacitance of the SWNT@C micro-supercapacitor is also higher than reported previously.[38]

The relationships between areal capacitance and current density were calculated from the galvanostatic charge-discharge curves (see Figure S5b). The specific capacitance of the SWNT@CHI is 7.1 mF cm^{-2} at a current density of 0.05 mA cm^{-2}. For the SWNT@C yarn micro-supercapacitor, the specific capacitance is 37.1 mF cm^{-2} at the same current density. Even at the current density of 4.2 mA cm^{-2}, the specific capacitance is still as high as 15.9 mF cm^{-2}. Such superior performance of the SWNT@C yarn can be attributed to the material structure. The porous SWNT network of the as-prepared yarn provides a high surface area, and yarn structure ensures a short ion diffusion path. The SWNT@C based yarn micro-supercapacitors have c.a. 42.86% capacitance retention when the scan rate was increased from 0.05 to 4.2 mA cm^{-2}, which is much better than reported in the literature.[39]

ADVANCED MATERIALS
www.advmat.de

www.MaterialsViews.com

For the as-prepared yarn micro-supercapacitors, the series resistance arises from the resistance of yarn electrode and electrolyte. The electrical conductivities of SWNT@C yarn (c.a. 601.8 S cm^{-1}) electrode is much higher than SWNT@CHI yarn (c.a. 38.98 S cm^{-1}). As shown in Figure 3e, the Nyquist plots of both materials suggest excellent capacitor behavior. For practical applications, cycling stability was a significant factor. The long-term cycling stability of yarn micro-supercapacitors were evaluated through the galvanostatic charge-discharge process conducted at 0.5 mA cm^{-2} (Figure 3f). The SWNT@C yarn shows c.a. 1.50% of capacitance loss after 10,000 cycles. While for the SWNT@CHI yarn, the capacitance increases by 1.07% after the same test cycles owing to the osmosis of electrolyte through the shell of CHI on the surface of the SWNT yarn. Such high electrochemical performance of as-prepared SWNT@C micro-supercapacitor is attributed to the fine combination of activated carbon and SWNT. The appropriate content of activated carbon adhesions to SWNT greatly contribute to the overall improvement of performance, and little effect on the electrical conductivities of SWNT. The partial enlarged image of Figure 3e is shown in Figure S5c. The x-intercept of Nyquist plots represents the equivalent series resistance (ESR) for two-electrode supercapacitors. The ESR of micro-scale solid-state fiber supercapacitors is commonly larger than the normal supercapacitor devices. Firstly, the main reason is that there is no extra metal current collector in the device. The efficiency of current collecting remains lower compared with a metal film current collector. Secondly, the solid-electrolytes also bring charge-transfer issues compared with liquid electrolytes. Such as, the interface resistance between electrodes and electrolytes increases a lot and the solid-electrolyte is difficult to diffuse into the electrode inner layer. However, we can see clearly from the figure S5c, the ESR of SWNT@CHI and SWNT@C are 944 Ω and 163 Ω, respectively. The value of SWNT@C yarn based micro-supercapacitor (163 Ω) is much smaller than that in metal-free electrode in a previous report.[38]

The ragone plots of areal and volumetric energy and power densities for the yarn micro-supercapacitors are compared with that reported in the literature. **Figure 4** shows the volumetric energy and power densities, and the corresponding areal energy and power densities are given as Figure S5d. Both the volumetric and areal energy densities have been significantly improved after carbonization. The areal energy density varied from 3.29 (for SWNT@C) to 1.41 (for SWNT@CHI) μWh cm^{-2} in the power density range of 40 to 3360 μW cm^{-2}. This performance is much better than reported previously.[40] Besides, as seen clearly from Figure 4, the volumetric energy density varied from 3.7 to 1.6 mWh cm^{-3} in a power density range of 45.7 to 3840 mW cm^{-3}, which is higher than the state of the art onion-like carbon[15] and graphene-based supercapacitors.[16] The obtained high energy and power density in our work can be attributed to the large effective area for ion storage within the porous structure and the high conductivity of the SWNT@C yarn.

A single yarn micro-supercapacitor shows exceptional electrochemical performance, which makes it promising for micro-electronics. However, the current and potential range offered by a single yarn micro-supercapacitor cannot meet the power and energy requirement of practical microelectronics. The problem may well be resolved just by integration of the yarn micro-supercapacitors in series, or in parallel. **Figures 5**a & c show four of yarn micro-supercapacitor units connected together in parallel and in series configurations. On the substrate of polytetrafluoroethylene (PTFE) paper, the yarn micro-supercapacitors can be bended and show exceptional flexibility. From the CV curves in Figure 5b, the output current (four in parallel assembly) increases by a factor of four with the same voltage window of 0 to 0.8 V. For the four in series assembly in Figure 5d, the voltage window can be enlarged to 3.2 V, whereas the unit can only operates below 0.8 V. The ESR of micro-supercapacitors connected in series and in parallel are shown in Figure S6. The demonstration of micro-supercapacitors connected in series powering a light-emitting diode (LED) is shown in **Figures 6**a & b. The device can be charged by a conventional silicon solar cell, and then provide adequate energy to light the LED which consumes high power for lighting.

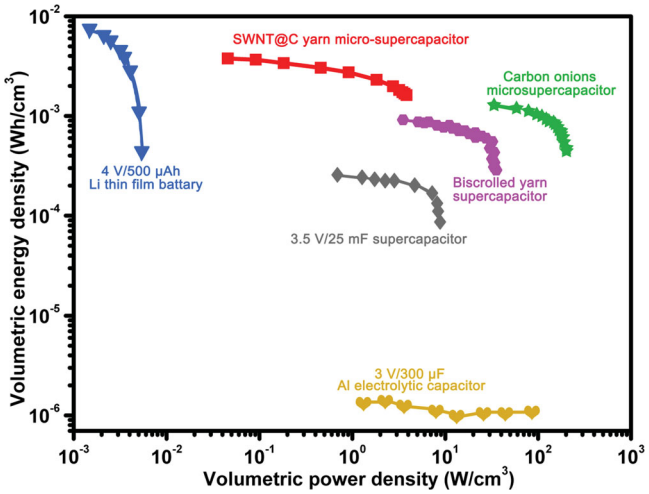

Figure 4. Specific power density against specific energy for yarn micro-supercapacitors. Ragone plot of the 4 V/500 μAh Li ion thin film battary, 3.5 V/25 mF supercapacitor and carbon onions microsupercapacitor are obtained from Ref. [15]. Besides, the rogone plot of the 3 V/300 μF Al electrolytic capacitor and biscrolled yarn supercapacitor are obtained from Ref. [16] and Ref. [6], respectively.

Flexible, deformable and micro-scale supercapacitors are indispensable for energy storage devices in microelectronics. Here, we demonstrate a high-performance yarn micro-supercapacitor with single-walled carbon nanotubes and activated carbon electrodes. The fine combination of single-walled carbon nanotubes and activated carbon provides the yarn micro-supercapacitors with more effective area for ion transportation and energy storage. The capacitance is 48.5 F cm^{-3} (74.6 F g^{-1}) at a scan rate of 2 mV s^{-1}, 42.4 F cm^{-3} (65.2 F g^{-1}) at a current density of 0.05 mA cm^{-2}. Besides, the energy density reaches 3.7 mWh cm^{-3} at a power density of 45.7 mW cm^{-3}, which are much higher than that reported previously. The device shows high stability retaining 98.5% of the capacitance after 10,000 charge-discharge cycles. Such micro-supercapacitors of high capacitance, energy density and cycling stability hold great promise for applications in microelectronics.

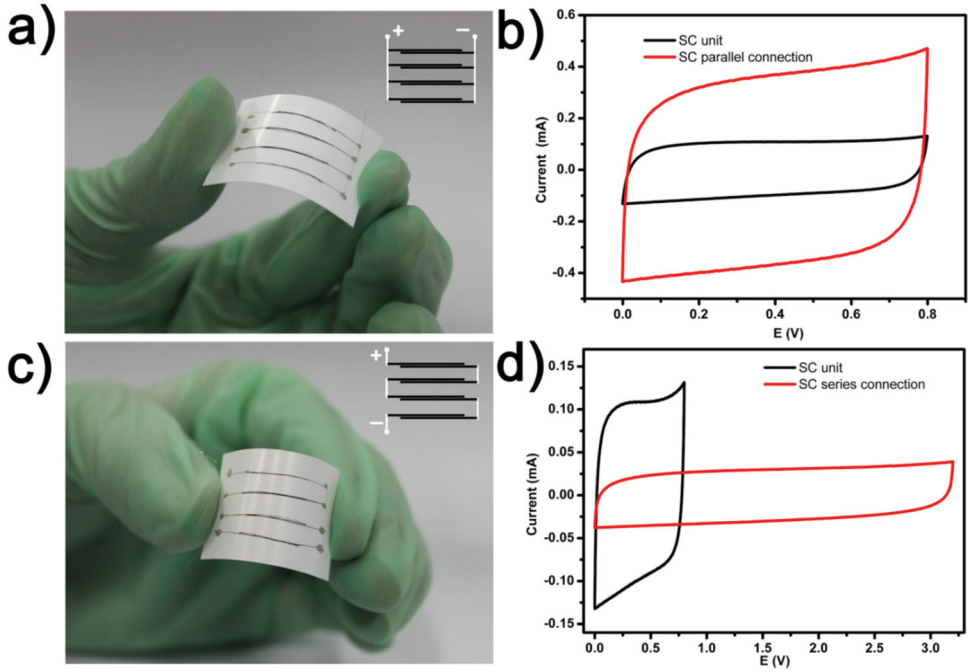

Figure 5. The electrochemical performance of the yarn micro-supercapacitors in series and parallel. a) Four units in parallel (insert image is the parallel connection diagram of supercapacitors). b) Cyclic voltammograms of the unit and parallel circuit. c) Four units in series (insert image is the in series connection diagram of supercapacitors). d) Cyclic voltammograms of the unit and in series circuit.

Experimental Section

Preparation of Spinning Dispersions and CHI Solution: SWNT and SDC were mixed in a mass ratio of 1.5:1, and then de-ionized water was added. After a low power ultrasonic treatment in ultrasonic cleaning machine for 10 min, the SWNT dispersion was treated by probe-sonication using 200 W for 2 h. The concentration of SWNT was 4 mg mL^{-1}. As to CHI solution, the CHI powders were added to 1% acetic acid under vigorous stirring.

Preparation of Yarn Electrode: Spinning dispersion and CHI solution were loaded in two syringes. Under the drive of the dual syringe pump, spinning dispersion and CHI solution flew in the glass tube. Once the spinning dispersion contacted with CHI solution, it coagulated from surface to interior and formed a yarn. Then, the SWNT@CHI yarns were transferred to a tube furnace, and heated for 2 h at 600 °C under the nitrogen atmosphere. This was followed by washing in concentrated nitric acid and de-ionized water.

Fabrication of Yarn Micro-Supercapacitors: 1 mL of H_2SO_4 and 1 g PVA powder were added to 10 mL de-ionized water with vigorous stirring at 85 °C. Two yarns were coated with a layer of gel electrolyte and clung close.

Characterization and Instrumentation: The dispersed state of SWNT was tested by Transmission Electron Microscopy (TEM, Tecnai G220 S-TWIN). The microstructures of the SWNT dispersion, SWNT@CHI and SWNT@C yarns were investigated by field emission Scanning Electron Microscopy (SEM, Hitachi S-4800, Japan). Raman spectroscopy (Renishaw inVia plus, UK), X-ray photoelectron spectroscopy (XPS, ESCALAB250Xi, USA), BET (Micromeritics Tristar II 3020) and Dynamic Mechanical Analyzer (Q800), were also carried out to analyze the structures and mechanical performance of the SWNT samples and yarns. CV, EIS, and galvanostatic charge-discharge measurements were performed to evaluate the electrochemical performance by a potential static electrochemical workstation (VMP3, Bio-Logic, France).

Supporting Information

Supporting Information is available from the Wiley Online Library or from the author.

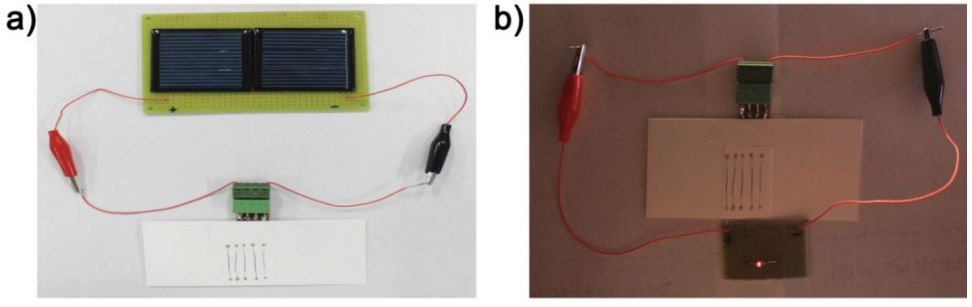

Figure 6. Potential application of yarn micro-supercapacitors. a) Solar cells charging for the device (Five yarn micro-supercapacitors units were connected in series). b) The device could power a red light-emitting diode independently.

ADVANCED MATERIALS
www.advmat.de

www.MaterialsViews.com

Acknowledgements

This work was supported by the Ministry of Science and Technology of China (Grant Nos. 2010DFB63530 and 2011CB932300) the National Natural Science Foundation of China (Grant Nos. 21125420 and 20974029), and the Chinese Academy of Sciences.

Received: January 25, 2014
Revised: March 1, 2014
Published online: April 1, 2014

[1] R. F. Service, *Science* **2003**, *301*, 909.
[2] D. De Rossi, *Nat. Mater.* **2007**, *6*, 328.
[3] T. Chen, L. B. Qiu, Z. B. Yang, Z. B. Cai, J. Ren, H. P. Li, H. J. Lin, X. M. Sun, H. S. Peng, *Angew. Chem. Int. Ed.* **2012**, *51*, 11977.
[4] K. Jost, D. Stenger, C. R. Perez, J. K. McDonough, K. Lian, Y. Gogotsi, G. Dion, *Energy Environ. Sci.* **2013**, *6*, 2698.
[5] V. T. Le, H. Kim, A. Ghosh, J. Kim, J. Chang, Q. A. Vu, D. T. Pham, J. H. Lee, S. W. Kim, Y. H. Lee, *ACS Nano* **2013**, *7*, 5940.
[6] J. A. Lee, M. K. Shin, S. H. Kim, H. U. Cho, G. M. Spinks, G. G. Wallace, M. D. Lima, X. Lepro, M. E. Kozlov, R. H. Baughman, S. J. Kim, *Nat. Commun.* **2013**, *4*, 1970.
[7] B. Liu, D. S. Tan, X. F. Wang, D. Chen, G. Z. Shen, *Small* **2013**, *9*, 1998.
[8] K. Wang, Q. H. Meng, Y. J. Zhang, Z. X. Wei, M. H. Miao, *Adv. Mater.* **2013**, *25*, 1494.
[9] S. W. Lee, N. Yabuuchi, B. M. Gallant, S. Chen, B. S. Kim, P. T. Hammond, Y. Shao-Horn, *Nat. Nanotechnol.* **2010**, *5*, 531.
[10] M. F. L. De Volder, S. H. Tawfick, R. H. Baughman, A. J. Hart, *Science* **2013**, *339*, 535.
[11] D. N. Futaba, K. Hata, T. Yamada, T. Hiraoka, Y. Hayamizu, Y. Kakudate, O. Tanaike, H. Hatori, M. Yumura, S. Iijima, *Nat. Mater.* **2006**, *5*, 987.
[12] K. L. Jiang, Q. Q. Li, S. S. Fan, *Nature* **2002**, *419*, 801.
[13] N. Behabtu, C. C. Young, D. E. Tsentalovich, O. Kleinerman, X. Wang, A. W. K. Ma, E. A. Bengio, R. F. ter Waarbeek, J. J. de Jong, R. E. Hoogerwerf, S. B. Fairchild, J. B. Ferguson, B. Maruyama, J. Kono, Y. Talmon, Y. Cohen, M. J. Otto, M. Pasquali, *Science* **2013**, *339*, 182.
[14] A. B. Dalton, S. Collins, E. Munoz, J. M. Razal, V. H. Ebron, J. P. Ferraris, J. N. Coleman, B. G. Kim, R. H. Baughman, *Nature* **2003**, *423*, 703.
[15] D. Pech, M. Brunet, H. Durou, P. H. Huang, V. Mochalin, Y. Gogotsi, P. L. Taberna, P. Simon, *Nat. Nanotechnol.* **2010**, *5*, 651.
[16] M. F. El-Kady, V. Strong, S. Dubin, R. B. Kaner, *Science* **2012**, *335*, 1326.
[17] H. J. Lin, L. Li, J. Ren, Z. B. Cai, L. B. Qiu, Z. B. Yang, H. S. Peng, *Sci. Rep.* **2013**, *3*, 1353.
[18] A. Laforgue, P. Simon, J. F. Fauvarque, *Synth. Met.* **2001**, *123*, 311.
[19] P. Simon, Y. Gogotsi, *Nat. Mater.* **2008**, *7*, 845.
[20] M. Beidaghi, C. L. Wang, *Electrochim. Acta* **2011**, *56*, 9508.
[21] D. Belanger, X. M. Ren, J. Davey, F. Uribe, S. Gottesfeld, *J. Electrochem. Soc.* **2000**, *147*, 2923.
[22] Y. Gogotsi, P. Simon, *Science* **2011**, *334*, 917.
[23] P. Poulin, B. Vigolo, P. Launois, *Carbon* **2002**, *40*, 1741.
[24] M. K. Shin, B. Lee, S. H. Kim, J. A. Lee, G. M. Spinks, S. Gambhir, G. G. Wallace, M. E. Kozlov, R. H. Baughman, S. J. Kim, *Nat. Commun.* **2012**, *3*, 650.
[25] F. Gao, L. Viry, M. Maugey, P. Poulin, N. Mano, *Nat. Commun.* **2010**, *1*, 2.
[26] B. Vigolo, A. Penicaud, C. Coulon, C. Sauder, R. Pailler, C. Journet, P. Bernier, P. Poulin, *Science* **2000**, *290*, 1331.
[27] J. Zawadzki, H. Kaczmarek, *Carbohydr. Polym.* **2010**, *80*, 394.
[28] A. Kucinska, A. Cyganiuk, J. P. Lukaszewicz, *Carbon* **2012**, *50*, 3098.
[29] Y. H. Yang, J. H. Cui, M. T. Zheng, C. F. Hu, S. Z. Tan, Y. Xiao, Q. Yang, Y. L. Liu, *Chem. Commun.* **2012**, *48*, 380.
[30] Z. G. Wu, W. Feng, Y. Y. Feng, Q. Liu, X. H. Xu, T. Sekino, A. Fujii, M. Ozaki, *Carbon* **2007**, *45*, 1212.
[31] H. Ago, T. Kugler, F. Cacialli, W. R. Salaneck, M. S. P. Shaffer, A. H. Windle, R. H. Friend, *J. Phys. Chem. B* **1999**, *103*, 8116.
[32] Y. Wang, C. A. Di, Y. Q. Liu, H. Kajiura, S. H. Ye, L. C. Cao, D. C. Wei, H. L. Zhang, Y. M. Li, K. Noda, *Adv. Mater.* **2008**, *20*, 4442.
[33] L. Li, Z. Y. Qin, X. Liang, Q. Q. Fan, Y. Q. Lu, W. H. Wu, M. F. Zhu, *J. Phys. Chem. C* **2009**, *113*, 5502.
[34] T. M. Wu, Y. W. Lin, C. S. Liao, *Carbon* **2005**, *43*, 734.
[35] H. S. Fan, H. Wang, N. Zhao, X. L. Zhang, J. Xu, *J. Mater. Chem.* **2012**, *22*, 2774.
[36] M. D. Stoller, S. J. Park, Y. W. Zhu, J. H. An, R. S. Ruoff, *Nano Lett.* **2008**, *8*, 3498.
[37] M. F. El-Kady, R. B. Kaner, *Nat. Commun.* **2013**, *4*, 1475.
[38] X. Chen, L. Qiu, J. Ren, G. Guan, H. Lin, Z. Zhang, P. Chen, Y. Wang, H. Peng, *Adv. Mater.* **2013**, *25*, 6436.
[39] X. Li, T. Zhao, Q. Chen, P. Li, K. Wang, M. Zhong, J. Wei, D. Wu, B. Wei, H. Zhu, *Phys. Chem. Chem. Phys.* **2013**, *15*, 17752.
[40] Y. P. Fu, X. Cai, H. W. Wu, Z. B. Lv, S. C. Hou, M. Peng, X. Yu, D. C. Zou, *Adv. Mater.* **2012**, *24*, 5713.